HHS Public Access

Author manuscript

Nat Chem. Author manuscript; available in PMC 2012 May 01.

Published in final edited form as:

Nat Chem. ; 3(11): 868–874. doi:10.1038/nchem.1163.

In Situ Quantitative Imaging of Cellular Lipids Using Molecular Sensors

Youngdae Yoon[1], **Park J. Lee**[1], **Svetlana Kurilova**, and **Wonhwa Cho**

Department of Chemistry, University of Illinois at Chicago, Chicago, IL 60607, USA

Abstract

Membrane lipids are dynamic molecules that play important roles in cell signaling and regulation but an *in situ* imaging method for quantitatively tracking lipids in living cells is lacking at present. Here we report a new chemical method of quantitative lipid imaging using sensors engineered by labeling proteins with an environmentally sensitive fluorophore. A prototype sensor for phosphatidylinositol-4,5-bisphosphate (PtdIns(4,5)P_2)– a key signaling lipid in diverse cellular processes–was generated by covalently attaching a single 2-dimethylamino-6-acyl-naphthalene group to the N-terminal α-helix of the engineered epsin1 ENTH domain– a protein that selectively binds PtdIns(4,5)P_2. The sensor allows robust and sensitive *in situ* quantitative imaging in mammalian cells, providing new insight into the spatiotemporal dynamics and fluctuation of this key signaling lipid. Application of the sensor to immune cells reveals the presence of a local threshold PtdIns(4,5)P_2 concentration required for triggering phagocytosis. This sensor strategy is generally applicable to *in situ* quantification of other cellular lipids.

INTRODUCTION

Many membrane lipids such as phosphoinositides and sphingolipids control diverse cellular processes, including cell proliferation, apoptosis, metabolism and migration, by regulating the localization, activities, and mutual interactions of their effector proteins[1,2]. These lipids and their downstream targets constitute complex signaling networks and perturbations in these networks contribute to the pathogenesis of human diseases including inflammation, cancer, diabetes and metabolic diseases[3]. Since lipids are dynamic molecules that are continuously produced, degraded, and transported in a tightly controlled manner[4] and their local concentrations may serve as thresholds for triggering diverse cellular processes, determination of their concentrations in a spatiotemporally resolved manner is a key step toward the understanding of growing myriad of lipid-mediated biological processes and the

[2]Corresponding author: Wonhwa Cho, Department of Chemistry, University of Illinois at Chicago, Chicago, IL 60607, USA; wcho@uic.edu.

[1]These authors contributed equally to this work.

SUPPLEMENTAL INFORMATION

Supplemental information includes a table, eleven figures, extended methods, a movie, and references.

AUTHOR CONTRIBUTIONS

W.C. and Y.Y. conceived the lipid sensor strategy. W.C. supervised the project and Y.Y. designed and prepared the sensor. P.J.L. and S.K. performed all microscopy imaging and image analysis.

development of new strategies to diagnose, treat, and prevent human diseases caused by dysfunctional membrane-associated processes. Despite various efforts, however, real-time *in situ* lipid quantification in live cells remains technically challenging partly because lipids exist not as mono-dispersed entity but as part of large aggregates, such as cell membranes.

Many membrane lipids that play cellular regulatory roles are selectively recognized by cellular proteins containing modular lipid binding domains[5,6]. Thus, lipid binding domains tagged with a fluorescence protein (or two for fluorescence resonance energy transfer analysis), such as green fluorescence protein, have been widely used to visualize the spatiotemporal dynamics of various cellular lipids[7,8]. Although these genetically incorporated probes offer experimental convenience, they can provide only semi-quantitative information due to inherent problems, including calibration difficulty, high background, and low sensitivity[7,9]. Furthermore, lipid sensors made of naturally occurring lipid binding domains present many practical problems because of their relatively low lipid specificity and affinity as well as potential interaction with other cellular proteins[9]. Although mass spectrometry-based lipid analysis[10,11] offers high sensitivity, the current technology still requires physical separation of lipids from cells and thus can provide neither spatial nor real-time temporal information.

To overcome the limitations of current lipid analysis methods, we developed a new strategy that employs protein engineering and chemical incorporation of a fluorescence probe. Specifically, a lipid binding protein module is first engineered for optimal lipid binding properties and minimal affinity for cellular proteins and the engineered protein is then converted into a “turn-on” fluorescence nanosensor by single-site chemical labeling with an environment-sensitive fluorophore that exhibits a large increase in fluorescence upon lipid binding. As a prototype, we generated a specific sensor for phosphatidylinositol-4,5-bisphosphate (PtdIns(4,5)P_2) that has been implicated in numerous cellular processes, including cell signaling, membrane remodeling, and regulation of membrane proteins and cytoskeletons[12–14]. It has been reported that PtdIns(4,5)P_2 is present mainly in the plasma membrane (PM) as a minor component (i.e., ≈1%)[12–14]; however, its actual concentration, distribution, and spatiotemporal fluctuation has not been quantitatively determined[14–16]. In particular, although local enrichment of PtdIns(4,5)P_2 in the PM has been supported by recent reports[17,18], spatiotemporal resolution of local PtdIns(4,5)P_2 heterogeneity has not been quantitatively achieved. Also, a possibility that the local PtdIns(4,5)P_2 concentration may serve as variable thresholds for different processes has not been explored. Here we show that the new sensor allows direct PtdIns(4,5)P_2 quantification in a spatiotemporally resolved manner in live cells, providing new insight into complex PtdIns(4,5)P_2-mediated biological processes.

RESULTS

PtdIns(4,5)P_2 Sensor Protein Engineering

Unlike those proteins that interact with soluble ligands, lipid binding domains and proteins must first interact with the membrane surface for specific lipid recognition because all lipids are present in the membrane[5]. Thus, they typically have a membrane binding surface as well as a lipid binding groove[5] and the optimization of their lipid binding properties would

involve engineering of both sites. Among a number of lipid binding domains that are known to bind PtdIns(4,5)P_2 with relatively high specificity, we selected the ENTH domain of epsin1[19–21] as a template for sensor protein engineering because of its favorable membrane binding properties. It should be noted that the PH domain of phospholipase Cδ (PLCδ-PH) tagged with a fluorescent protein has been most commonly used as a cellular PtdIns(4,5)P_2 probe[7–9]. As documented in the literature[7–9] and confirmed by our surface plasmon resonance (SPR) analysis (Table S1 and Fig. S1), however, this PH domain also binds inositol-(1,4,5)-triphosphate (Ins(1,4,5)P_3), phosphatidylinositol-3,4-bisphosphate (PtdIns(3,4)P_2) and phosphatidylinositol-3,4,5-trisphosphate (PtdIns(3,4,5)P_3) with high affinity, which can complicate PtdIns(4,5)P_2 quantification under physiological conditions. The ENTH domain shows much better selectivity for PtdIns(4,5)P_2 over Ins(1,4,5)P_3 (Fig. S1). Although it still has residual affinity for PtdIns(3,4)P_2 and PtdIns(3,4,5)P_3 (Table S1), this residual affinity can be readily suppressed by protein engineering (see below), which turned out to be much more difficult for PLCδ-PH. Furthermore, the ENTH domain shows much faster membrane association and dissociation than the PH domain (Table S1 and Fig. S1), which is critical for time-resolved lipid quantification. To further improve the PtdIns(4,5)P_2 specificity and the overall membrane affinity of the ENTH domain, we mutated Ser-4 (Fig. 1a) that is located near both the membrane binding surface and the lipid binding pocket and thus likely to be involved in both specific lipid headgroup recognition and the non-specific interaction with the membrane surface. When Ser-4 was mutated to Trp, Tyr, Val, or Ala, all mutants showed better PtdIns(4,5)P_2 specificity than the wild type (see Table S1 for data on two mutants, S4W and S4Y), while showing a range of affinity for PtdIns(4,5)P_2-containing membranes, suggesting that each of them can be used as a PtdIns(4,5)P_2 sensor that covers a different concentration range. In this study we primarily used the Ser-4 to Trp (S4W) mutant because its K_d value for PtdIns(4,5)P_2 in terms of mole % in the vesicles (see Fig. 2a and Fig. S3) is closest to the estimated cellular concentration of PtdIns(4,5)P_2 (i.e., 1%)[12–14].

Generation and Spectral Properties of the Fluorescence Turn-On Sensor

Our strategy for converting an optimized lipid binding domain into a fluorescence “turn-on” sensor is to chemically introduce to the protein an organic fluorophore that shows either a dramatic increase (preferably from a negligible background) in fluorescence emission intensity at a given wavelength or a large spectral shift upon binding a lipid in the membrane. This hybrid molecular sensor can then be used for single-wavelength or ratiometric fluorescence analysis for lipid quantification. Since the membrane-binding surface of a protein experiences a large environmental change from a polar aqueous surrounding to a non-polar lipid environment, we reasoned that a polarity-sensitive fluorophore attached to the membrane-binding surface would display desired spectral properties upon membrane and lipid binding. We therefore further engineered the ENTH domain to introduce a single labeling site (M10C) on the membrane binding surface[19,20] while removing an endogenous Cys (C96A) (Fig. 1a). These two mutations exerted a relatively minor effect on the membrane affinity of both wild type and S4W (Table S1).

Various polarity-sensitive fluorophores, including 2-dimethylamino-6-acyl-naphthalene (DAN), Nile red, 7-nitrobez-2-oxa-1,3-diazole (NBD), 1-Anilinonaphthalene-8-sulfonyl

(ANS), and 5-dimethylaminonaphthalene-1-sulfony (dansyl) groups, have been reported but our selection is limited to those fluorophores that can effectively partition into the membrane because of our sensor design. Examination of spectral and membrane binding properties of these fluorophores suggested that the DAN group (Fig. 1a) is ideally suited for lipid sensor application: i.e., it was reported to readily partition into the membrane and exhibit a large fluorescence blue shift when transferred from aqueous to non-polar environment[22]. We thus chemically labeled the engineered protein (i.e., S4W/M10C/C96A: *eENTH*) with the DAN group using commercially available acrylodan. The resulting sensor, *DAN-eENTH* has ca. 12-fold higher affinity for PtdIns(4,5)P_2-containing vesicles than the wild type and excellent PtdIns(4,5)P_2 specificity (Table S1). The enhanced PtdIns(4,5)P_2 affinity by DAN labeling helps expand the dynamic range to lower PtdIns(4,5)P_2 concentrations. Furthermore, unlike the wild type ENTH domain, *DAN-eENTH* showed no tendency to induce membrane deformation even at a high concentration (e.g., 10 μM) (Fig. S2).

To check the feasibility of PtdIns(4,5)P_2 quantification using *DAN-eENTH*, we first measured its spectral change upon membrane binding by spectrofluorometry. As shown in Fig. 1b, *DAN-eENTH* exhibited a dramatic blue shift upon binding to PtdIns(4,5)P_2-containing large unilamellar vesicles (LUV), i.e., 1-palmitoyl-2-oleoyl-*sn*-3-phosphocholine (POPC)/1-palmitoyl-2-oleoyl-*sn*-3-phosphoserine (POPS)/PtdIns(4,5)P_2 (80-*x*:20:*x* with *x* = 0–3 mole%), and the maximal increase in emission intensity (*F*) at 460 nm (F_{460}) depended on the PtdIns(4,5)P_2 concentration ([PtdIns(4,5)P_2]) in LUV. The blue shift is presumably due to the partial insertion of the environmentally sensitive DAN probe attached to the membrane binding surface of the ENTH domain into the low dielectric interior of the membrane[22]. *DAN-eENTH* showed negligible binding to LUV containing any other phosphoinositide (Fig. S3a), again demonstrating high specificity. This favorable spectral change of *DAN-eENTH* suggests that [PtdIns(4,5)P_2] can be determined either by intensity analysis at a single wavelength (e.g., F_{450}; see Fig. S3b) or by ratiometric analysis at two wavelengths (e.g., F_{450}/F_{520}; see Fig. S3c).

To calibrate *DAN-eENTH* for cellular PtdIns(4,5)P_2 quantification, we then added *DAN-eENTH* to the giant unilamellar vesicles (GUV) made of POPC/POPS/PtdIns(4,5)P_2 (80-*x*:20:*x*) and measured the *F* values using a two-photon microscope (Fig. S4a). In this case, 436 ± 10 (for blue channel; F_B) and the 525 ± 25 (for green channel; F_G) band pass filters, respectively, were used to spectrally separate the *F* values of the membrane-bound and the free *DAN-eENTH* species (see Methods). Even at the highest [PtdIns(4,5)P_2] employed, both F_B and F_B/F_G remained constant regardless of [*DAN-eENTH*] as long as [*DAN-eENTH*] > 25 nM (Fig. S4b), indicating that both the single channel and the ratiometric analysis can be used effectively for PtdIns(4,5)P_2 quantification. Under our conditions, F_B that originates exclusively from lipid-bound *DAN-eENTH* (i.e., the signal detectable only at the membrane) was negligible in the absence of PtdIns(4,5)P_2, making background correction unnecessary. The resulting F_B versus the surface concentration of PtdIns(4,5)P_2 ($[PtdIns(4,5)P_2]_s$; see Supplementary Methods for its calculation) (Fig. 2a) or (F_B/F_G) versus $[PtdIns(4,5)P_2]_s$ (Fig. 2b) calibration curve was used for ensuing PtdIns(4,5)P_2 quantification in GUV and in mammalian cells. The lateral spatial resolution of conventional light microscope is limited by the diffraction limit (≈250 nm for green light excitation). We thus typically divided the

circumference of the GUV or PM (≈31 μm for a GUV or a cell with 10 μm diameter) into 360 degrees and integrated the photon count data for every three degrees (≈261 nm). The temporal resolution of our sensor technology depends on the sensitivity of the detector and the speed of scanner and can reach the order of second with a conventional photomultiplier tube.

Cellular PtdIns(4,5)P_2 Quantification

We delivered *DAN-eENTH* into NIH 3T3 cells by microinjection for live cell imaging. The green channel (Fig. 3a) representing both PtdIns(4,5)P_2-bound and free *DAN-eENTH* illustrates that the sensor was successfully loaded into cells and distributed in the cytosol and the PM. Also, the blue channel (Fig. 3b and Fig. S5a) representing PtdIns(4,5)P_2-bound *DAN-eENTH* shows that cellular PtdIns(4,5)P_2 was highly enriched in the PM, consistent with previous reports[12–14]. When a *DAN-eENTH* mutant devoid of PtdIns(4,5)P_2 affinity (see Table S1) was injected, it was mainly localized in the cytosol (see Fig. S5b). This precludes a possibility that the PM localization of *DAN-eENTH* is driven primarily by binding to proteins on the PM. *DAN-eENTH* did not translocate to the nucleus when microinjected to the cytosol because it does not have the nuclear localization sequence; however, when it was directly microinjected into the nucleus (or both the cytosol and the nucleus), PtdIns(4,5)P_2 was detected in the nuclear membrane and within the nucleus (Fig. S5c). For this investigation, we focused on PtdIns(4,5)P_2 in the PM that was detected by *DAN-eENTH* injected into the cytosol. Lastly, it should be noted that *DAN-eENTH* can also be successfully delivered to mammalian cells, including NIH 3T3 cells, by a liposome-based protein delivery system, BioPORTER™ (see Fig. S6); however, we preferentially used the microinjection for cell delivery because it allows a finer control of the amount of the sensor delivered to the cell.

We then determined $[\text{PtdIns}(4,5)P_2]_s$ in the PM in a time-dependent manner by either single-channel (F_B) or ratiometric (F_B/F_G) analysis using the calibration curve (Fig. 2a or 2b; see detailed description in Supplementary Methods). At a given time, dramatic spatial heterogeneity of $[\text{PtdIns}(4,5)P_2]_s$ was visible (Fig. 3c) with local $[\text{PtdIns}(4,5)P_2]_s$ varying from negligible to >80 *nmole*/m^2. Also, the local $[\text{PtdIns}(4,5)P_2]_s$ rapidly fluctuated over time (see Fig. S7a, Fig. S7c and MovieS1) throughout the PM, demonstrating spatiotemporal heterogeneity and fluctuation. Despite local heterogeneity of PtdIns(4,5)P_2 at a given time, $[\text{PtdIns}(4,5)P_2]_s$ averaged over 20 minutes displayed relatively homogenous spatial distribution (Fig. S7b) with an average of 40 (±15) *nmole*/m^2. Assuming that a NIH 3T3 cell is a sphere with 10 μm radius (see Methods), this surface concentration corresponds to 17 μM in bulk cellular concentration, which is comparable to the reported estimate[14]. This indicates that PtdIns(4,5)P_2 shows a large degree of spatiotemporal heterogeneity and fluctuation although its overall concentration in the PM remains relatively constant. Spatial heterogeneity and temporal fluctuation of PtdIns(4,5)P_2 in the PM were observed in >85% of 43 NIH 3T3 and 30 MDCK cells effectively microinjected with *DAN-eENTH* (see some examples in Fig. S9) and >50% of NIH 3T3 cells to which *DAN-eENTH* was delivered by BioPORTER (Fig. S6). Spatiotemporally averaged (see above) $[\text{PtdIns}(4,5)P_2]_s$ for 10 randomly selected resting cells was 42 ± 6 *nmole*/m^2.

It has been reported that the change in membrane surface area caused by membrane trafficking and remodeling, such as ruffle formation, can contribute to a pseudo-change in lipid concentration when it is estimated from the fluorescence intensity of membrane associated fluorescence proteins[17,23]. The local heterogeneity and the temporal fluctuation of PtdIns(4,5)P_2 detected by our sensor should not be due to this surface area artifact because the ratiometric analysis is independent of the membrane surface area change. In fact, essentially the same results obtained from the ratiometric and the single-channel analyses in all our measurements preclude the possibility of the surface area artifact. Furthermore, inhibition of endocytosis or exocytosis had little effect on the phenomenon (see Fig. S8) and no significant increase in membrane surface area due to ruffle formation was detected under our experimental conditions. Lastly, although essentially all cells studied herein showed spatiotemporal heterogeneity and fluctuation of PtdIns(4,5)P_2, a considerable degree of variation was seen among cells (Fig. S9), again supporting that our findings are not due to systematic experimental artifacts.

To see if *DAN-eENTH* can also quantitatively monitor the agonist-induced changes in [PtdIns(4,5)P_2]$_s$, we treated NIH 3T3 cells with 1 μM insulin (Fig. S10b and Fig. S10c) or 1 mM ATP (Fig. S10d) and monitored the changes in [PtdIns(4,5)P_2]$_s$ in the PM. Insulin is known to stimulate phosphorylation of PtdIns(4,5)P_2 to PtdIns(3,4,5)P_3 by phosphoinositide 3-kinase[24] whereas ATP induces PtdIns(4,5)P_2 hydrolysis by PLC[25]; however, the extent of PtdIns(4,5)P_2 decrease by these treatments has not been accurately determined. Our quantification using *DAN-eENTH* shows that both treatments caused modest (i.e., ~10%) and reversible reduction in spatially averaged [PtdIns(4,5)P_2]$_s$ in the PM (Fig. S10c and Fig. S10d). Under the same conditions, insulin and ATP treatments partially and reversibly displaced PLCδ-PH-EGFP from the PM (Fig. S11). When cells were pre-treated with 300 nM of wortmannin, a phosphoinositide 3-kinase inhibitor, for 10 minutes (Fig. S10c) or 3 μM U73122, a PLC inhibitor, for 30 minutes (Fig. S10d), respectively, no detectable drop in [PtdIns(4,5)P_2]$_s$ was observed after insulin or ATP treatment, respectively. To show that our sensor can quantitatively monitor a rapid dynamic change of [PtdIns(4,5)P_2]$_s$ in the PM, we employed the rapamycin-induced PtdIns(4,5)P_2 depletion system in which rapamycin mediates the heterodimerization of the PM-anchored FRB domain of mTOR (PM-FRB) and the monomeric red fluorescence protein-FK506-binding protein 12-yeast inositol polyphosphate 5-phosphatase domain fusion protein (RF-Inp), resulting in the rapid PtdIns(4,5)P_2 hydrolysis in PM[26,27]. The addition of 2.5 μM rapamycin to NIH-3T3 cells co-transfected with PM-FRB, RF-Inp and PLCδ-PH-EGFP, resulted in fast dissociation of PLCδ-PH-EGFP from the PM (Fig. 4A), showing that PM translocation of RF-Inp causes spontaneous and quantitative hydrolysis of PtdIns(4,5)P_2 in the PM. Under the same conditions, our sensor microinjected into NIH-3T3 cells co-transfected with PM-FRB and RF-Inp was able to follow a rapid and extensive decrease in [PtdIns(4,5)P_2]$_s$ throughout the PM (Fig. 4B). Most important, our method allows for quantitative (i.e., ≈75% drop) determination of the [PtdIns(4,5)P_2]$_s$ decrease that cannot be achieved with PLCδ-PH-EGFP imaging.

Local PtdIns(4,5)P_2 Concentration as a Threshold for Triggering a Cellular Process

Having establish the methodology to quantitatively detect the local heterogeneity of and the agonist-induced change in PtdIns(4,5)P_2, we then tested the notion that the local PtdIns(4,5)P_2 concentration serves as a threshold for triggering a cellular process. As a pilot study, we determined the quantitative correlation between local $[PtdIns(4,5)P_2]_s$ and the extent of phagocytosis. The importance of local PtdIns(4,5)P_2 enrichment in the PM of phagocytic cells in the early stages of phagocytosis for actin polymerization and pseudopod extension has been well documented[17,28,29]. It was also reported that the enhanced level of PtdIns(4,5)P_2 in the region of the nascent phagosomes was required for phagocytosis[17]. However, direct quantification of PtdIns(4,5)P_2 during phagocytosis has not been reported. We microinjected the PtdIns(4,5)P_2 sensor to >50 macrophage J774A.1 cells that were allowed to make contact with apoptotic Jurkat T cells and determined $[PtdIns(4,5)P_2]_s$ in their PM while monitoring the progress of phagocytosis by differential interference contrast (DIC) imaging (Fig. 5). We found that for ≈40% of the macrophages, the local $[PtdIns(4,5)P_2]_s$ in the cell-cell contact region ranged from 60 to 80 $nmole/m^2$ (i.e., 70 ± 10) (Fig. 5a and 5b) and that these cells all successfully developed pseudopods surrounding Jurkat cells and completed the phagocytosis. Also, dramatic local enrichment of $[PtdIns(4,5)P_2]_s$ above 100 $nmole/m^2$ was seen in the extended pseudopods (Fig. 5c and 5d). However, the rest of macrophages with $[PtdIns(4,5)P_2]_s \leq 50$ $nmole/m^2$ throughout the contact region failed to develop PtdIns(4,5)P_2-enriched pseudopods (Fig. 5e to 5h). Together, these results clearly indicate the presence of the local threshold PtdIns(4,5)P_2 concentration (i.e., ≈60 $nmole/m^2$) in the initial cellular contact regions of phagocytic cells that is necessary for triggering actin polymerization and phagocytosis.

DISCUSSION

This work shows that our newly developed molecular sensor allows robust and sensitive *in situ* quantification of a key signaling lipid, PtdIns(4,5)P_2, in a spatiotemporally resolved manner under physiological conditions. The specific and sensitive PtdIns(4,5)P_2 quantification achieved using our sensor mainly derives from optimized membrane and lipid binding properties of the engineered ENTH domain and favorable spectral and membrane binding properties of the DAN probe. Strategic site-specific incorporation of the DAN probe into the membrane binding surface of the protein is also a critical factor as it greatly influences the degree of environmental change the probe experiences during lipid binding.

Spatiotemporally resolved PtdIns(4,5)P_2 quantification in mammalian cells provides new biological insight. Local enrichment of PtdIns(4,5)P_2 in the PM has been visualized for various cells actively undergoing membrane trafficking, most notably during phagocytosis[17,29], and for pheromone-activated yeast cells[18]. To our knowledge, however, our results represent the first quantitative spatiotemporal resolution of the local PtdIns(4,5)P_2 heterogeneity in resting cells. It has been recently reported that the local synthesis of PtdIns(4,5)P_2 by lipid kinases is critical for local PtdIns(4,5)P_2 enrichment in yeast cells[18]. Although further studies are needed to fully understand the mechanistic basis of the spatial heterogeneity of PtdIns(4,5)P_2 in mammalian cells, our result suggests that the PM in the resting state is primed for localized PtdIns(4,5)P_2-mediated processes. Most

important, our results support the notion that PtdIns(4,5)P_2 may control cellular processes by serving as local activation thresholds. This in turn raises an interesting possibility that PtdIns(4,5)P_2 (or other signaling lipids) may control diverse cellular processes differentially (and potentially coincidently) by serving as variable thresholds. Our sensor strategy should be generally applicable to quantification of other cellular lipids using engineered lipid binding domains specific for other lipids. Also, *in situ* quantification of multiple lipids, which can be achieved through the combinatorial use of different lipid binding domains and orthogonal fluorophores, should greatly help the systems-level understanding of numerous lipid-mediated cellular processes.

METHODS

Materials

Acrylodan (6-acryloyl-2-dimethylaminonaphthalene) and thrombin were purchased from Invitrogen. POPC and POPS were purchased from Avanti Polar Lipids. 1,2-dipalmitoyl derivatives of PtdIns(4,5)P_2, PtdIns(3,4,5)P_3, and other phosphoinositides were from Cayman Chemical. PM-FRB and RF-Inp constructs were generous gifts of Dr. Tamas Balla.

Protein Expression, Purification and Labeling

The Epsin1 ENTH domain (1-158 amino acids) was expressed as a C-terminal glutathione S-transferase (GST)-tagged protein. After purification by affinity chromatograph, its GST tag was removed by thrombin. Chemical labeling by acrylodan was performed on the GST-tagged protein bound to the GST-affinity column, followed by thrombin treatment and elution. The protein concentration was determined by Bradford assay (BioRad). The DAN labeling yield of *eENTH* was then calculated by determining moles of DAN (= absorbance at 391 nm/molar absorptivity of DAN at 391 nm (= 20,000 cm^{-1} M^{-1})) per mole of protein. The labeling step was repeated until >90% labeling yield was achieved.

In vitro Calibration and Determination of [PtdIns(4,5)P_2]

Hitachi F-4500 spectrofluorometer was used for all cuvette-based fluorescence measurements. *DAN-eENTH* (typically 500 nM) was added to POPC/POPS/PtdIns(4,5)P_2 (80-*x*:20:*x*) (*x* = 0–3 mole%) LUV prepared by extrusion and the emission spectra of DAN were measured with excitation wavelength set at 392 nm in a single-photon excitation mode. All fluorescence microscopy measurements were carried out at 37 °C in a two-photon excitation mode using the custom-built two-photon microscope that was described previously[30]. *In vitro* calibration of the *DAN-eENTH* sensor was performed with GUVs composed of POPC/POPS/PtdIns(4,5)P_2 (80-*x*:20:*x*) (*x* = 0–3 mole%). The *DAN-eENTH* was two-photon excited at 780 nm and 436 ± 10 (for blue channel; F_B) and the 525 ± 25 (for green channel; F_G) band pass filters, respectively, were used to spectrally separate the fluorescence emission of the membrane-bound and the free *DAN-eENTH* species. For the single-channel analysis, F_B versus $[PtdIns(4,5)P_2]_s$ data was fit using the equation: $F_B = (F_B)_{max}/(1 + K_d/[PtdIns(4,5)P_2]_s)$ and K_d and $(F_B)_{max}$ values were determined from non-linear least-squares analysis (see Fig. 2a). Then, $[PtdIns(4,5)P_2]_s$ from an unknown sample was calculated using the equation; $[PtdIns(4,5)P_2]_s = K_d F_B/((F_B)_{max} - F_B)$. For the ratiometric analysis, K_d and $(F_B/F_G)_{max}$ values were calculated from non-linear least-

squares analysis of the (F_B/F_G) versus $[PtdIns(4,5)P_2]_s$ plot using the equation; $(F_B/F_G) = (F_B/F_G)_{max}/(1 + K_d/[PtdIns(4,5)P_2]_s)$ and the theoretical calibration curve was constructed using these values (see Fig. 2b). Then, $[PtdIns(4,5)P_2]_s$ from an unknown sample was calculated using the equation; $[PtdIns(4,5)P_2]_s = K_d(F_B/F_G)/\{(F_B/F_G)_{max} - (F_B/F_G)\}$. For more detailed description, see Supplemental Methods.

Cellular [PtdIns(4,5)P_2] Determination

DAN-eENTH was delivered into NIH 3T3 cells grown in Dulbecco's modified Eagle's medium (DMEM) supplemented with 10% fatal bovine serum (FBS) by microinjection using the Eppendorf InjectMan NI 2 system. [*DAN-eENTH*] was adjusted to give strong enough F_B and F_G signals for robust data analysis. The cellular $[PtdIns(4,5)P_2]_s$ was determined from the observed (F_B/F_G) (ratiometric) or F_B (single channel) values using the *in vitro* calibration curves (Fig. 2a and 2b) determined for POPC/POPS/PtdIns(4,5)P_2 GUVs. The bulk cellular concentration of PtdIns(4,5)P_2 was estimated from $[PtdIns(4,5)P_2]_s$ assuming that a NIH 3T3 cell has a spherical shape with an average of 10 μm radius (i.e., $[PtdIns(4,5)P_2] = [PtdIns(4,5)P_2]_s \times$ (cell surface area/cell volume)). For the description of all inhibitor treatments of cells and rapamycin-induced PtdIns(4,5)P_2 depletion experiments, see Supplemental Methods.

Phagocytosis of Apoptotic Jurkat T Cells

Mouse macrophage cells J774A.1 were cultured in DMEM supplemented with 100 U/ml penicillin, 0.1 mg/ml streptomycin and 10% FBS, and plated on 8-well plates 1 day before the phagocytosis experiment. After *DAN-eENTH* was microinjected to J774A.1 cells, apoptotic Jurkat T cells, prepared by UV irradiation for 10 to 30 min, were added to the medium containing J774A.1 cells, the PtdIns(4,5)P_2 concentration was determined while the mixtures were incubated at 37 °C in a humidified atmosphere of 95 % air and 5 % CO_2.

SPR Analysis

All SPR measurements were performed at 23 °C in 20 mM Tris, pH 7.4, containing 0.16 M KCl using a lipid-coated L1 chip in the BIACORE X system as described previously[31]. LUVs of POPC/POPS/PtdIns(4,5)P_2 (or another phosphoinositide) (77:20:3) and POPC were used as the active surface and the control surface, respectively. Equilibrium SPR measurements were done at the flow rate of 5 μl/min to allow sufficient time for the *R* values of the association phase to reach near-equilibrium values. Sensorgrams were analyzed assuming a Langmuir-type binding between the protein (P) and protein binding sites (M) on vesicles (i.e., $P + M \leftrightarrow PM$), and the K_d value was determined by a nonlinear least-squares analysis. For kinetic SPR measurements, the flow rate was maintained at 15 μl/min for both association and dissociation phases.

Supplementary Material

Refer to Web version on PubMed Central for supplementary material.

Acknowledgments

This study was supported by a grant from National Institutes of Health (GM68849). It was also supported in part by the World Class University program R31-2008-000-10105-0 through the National Research Foundation of Korea funded by the Ministry of Education, Science and Technology and the Chicago Biomedical Consortium with support from the Searl Funds at the Chicago Community Trust. We thank Drs. Insan Kim, Sang-Yeob Kim, Surajit Bhattacharjee, Yasunori Kanaho, and Liang-Wei Gong for technical assistance in phagocytosis and membrane trafficking experiments. We also thank Dr. Tamas Balla for the generous gift of the PtdIns(4,5)-depletion system. Correspondence and requests for materials should be addressed to W.C.

References

1. Hannun YA, Obeid LM. Principles of bioactive lipid signalling: lessons from sphingolipids. Nat Rev Mol Cell Biol. 2008; 9:139–50. [PubMed: 18216770]
2. Cho W. Building signaling complexes at the membrane. Sci STKE. 2006; 2006:pe7. [PubMed: 16467194]
3. Wymann MP, Schneiter R. Lipid signalling in disease. Nat Rev Mol Cell Biol. 2008; 9:162–76. [PubMed: 18216772]
4. van Meer G, Voelker DR, Feigenson GW. Membrane lipids: where they are and how they behave. Nat Rev Mol Cell Biol. 2008; 9:112–24. [PubMed: 18216768]
5. Cho W, Stahelin RV. Membrane-protein interactions in cell signaling and membrane trafficking. Annu Rev Biophys Biomol Struct. 2005; 34:119–51. [PubMed: 15869386]
6. Lemmon MA. Membrane recognition by phospholipid-binding domains. Nat Rev Mol Cell Biol. 2008; 9:99–111. [PubMed: 18216767]
7. Varnai P, Balla T. Live cell imaging of phosphoinositide dynamics with fluorescent protein domains. Biochim Biophys Acta. 2006; 1761:957–67. [PubMed: 16702024]
8. Downes CP, Gray A, Lucocq JM. Probing phosphoinositide functions in signaling and membrane trafficking. Trends Cell Biol. 2005; 15:259–68. [PubMed: 15866030]
9. Irvine R. Inositol lipids: to PHix or not to PHix? Curr Biol. 2004; 14:R308–10. [PubMed: 15084300]
10. Han X, Gross RW. Global analyses of cellular lipidomes directly from crude extracts of biological samples by ESI mass spectrometry: a bridge to lipidomics. J Lipid Res. 2003; 44:1071–9. [PubMed: 12671038]
11. van Meer G. Cellular lipidomics. EMBO J. 2005; 24:3159–65. [PubMed: 16138081]
12. Di Paolo G, De Camilli P. Phosphoinositides in cell regulation and membrane dynamics. Nature. 2006; 443:651–7. [PubMed: 17035995]
13. McLaughlin S, Murray D. Plasma membrane phosphoinositide organization by protein electrostatics. Nature. 2005; 438:605–11. [PubMed: 16319880]
14. McLaughlin S, Wang J, Gambhir A, Murray D. PIP(2) and proteins: interactions, organization, and information flow. Annu Rev Biophys Biomol Struct. 2002; 31:151–75. [PubMed: 11988466]
15. van Rheenen J, Achame EM, Janssen H, Calafat J, Jalink K. PIP2 signaling in lipid domains: a critical re-evaluation. EMBO J. 2005; 24:1664–73. [PubMed: 15861130]
16. Hilgemann DW. Local PIP(2) signals: when, where, and how? Pflugers Arch. 2007; 455:55–67. [PubMed: 17534652]
17. Botelho RJ, et al. Localized biphasic changes in phosphatidylinositol-4,5-bisphosphate at sites of phagocytosis. J Cell Biol. 2000; 151:1353–68. [PubMed: 11134066]
18. Garrenton LS, Stefan CJ, McMurray MA, Emr SD, Thorner J. Pheromone-induced anisotropy in yeast plasma membrane phosphatidylinositol-4,5-bisphosphate distribution is required for MAPK signaling. Proc Natl Acad Sci U S A. 2010; 107:11805–10. [PubMed: 20547860]
19. Itoh T, et al. Role of the ENTH domain in phosphatidylinositol-4,5-bisphosphate binding and endocytosis. Science. 2001; 291:1047–51. [PubMed: 11161217]
20. Ford MG, et al. Curvature of clathrin-coated pits driven by epsin. Nature. 2002; 419:361–6. [PubMed: 12353027]

21. Stahelin RV, et al. Contrasting membrane interaction mechanisms of AP180 N-terminal homology (ANTH) and epsin N-terminal homology (ENTH) domains. J Biol Chem. 2003; 278:28993–9. [PubMed: 12740367]
22. Weber G, Farris FJ. Synthesis and spectral properties of a hydrophobic fluorescent probe: 6-propionyl-2-(dimethylamino)naphthalene. Biochemistry. 1979; 18:3075–8. [PubMed: 465454]
23. Terebiznik MR, et al. Elimination of host cell PtdIns(4,5)P(2) by bacterial SigD promotes membrane fission during invasion by Salmonella. Nat Cell Biol. 2002; 4:766–73. [PubMed: 12360287]
24. Ruderman NB, Kapeller R, White MF, Cantley LC. Activation of phosphatidylinositol 3-kinase by insulin. Proc Natl Acad Sci U S A. 1990; 87:1411–5. [PubMed: 2154747]
25. Rhee SG. Regulation of phosphoinositide-specific phospholipase C. Annu Rev Biochem. 2001; 70:281–312. [PubMed: 11395409]
26. Inoue T, Heo WD, Grimley JS, Wandless TJ, Meyer T. An inducible translocation strategy to rapidly activate and inhibit small GTPase signaling pathways. Nat Methods. 2005; 2:415–8. [PubMed: 15908919]
27. Varnai P, Thyagarajan B, Rohacs T, Balla T. Rapidly inducible changes in phosphatidylinositol 4,5-bisphosphate levels influence multiple regulatory functions of the lipid in intact living cells. J Cell Biol. 2006; 175:377–82. [PubMed: 17088424]
28. Swanson JA. Shaping cups into phagosomes and macropinosomes. Nat Rev Mol Cell Biol. 2008; 9:639–49. [PubMed: 18612320]
29. Grinstein S. Imaging signal transduction during phagocytosis: phospholipids, surface charge, and electrostatic interactions. Am J Physiol Cell Physiol. 2010; 299:C876–81. [PubMed: 20739621]
30. Stahelin RV, et al. Mechanism of diacylglycerol-induced membrane targeting and activation of protein kinase Cdelta. J Biol Chem. 2004; 279:29501–12. [PubMed: 15105418]
31. Manna D, et al. Differential roles of phosphatidylserine, PtdIns(4,5)P2, and PtdIns(3,4,5)P3 in plasma membrane targeting of C2 domains. Molecular dynamics simulation, membrane binding, and cell translocation studies of the PKCalpha C2 domain. J Biol Chem. 2008; 283:26047–58. [PubMed: 18621733]
32. Grynkiewicz G, Poenie M, Tsien RY. A new generation of Ca2+ indicators with greatly improved fluorescence properties. J Biol Chem. 1985; 260:3440–50. [PubMed: 3838314]

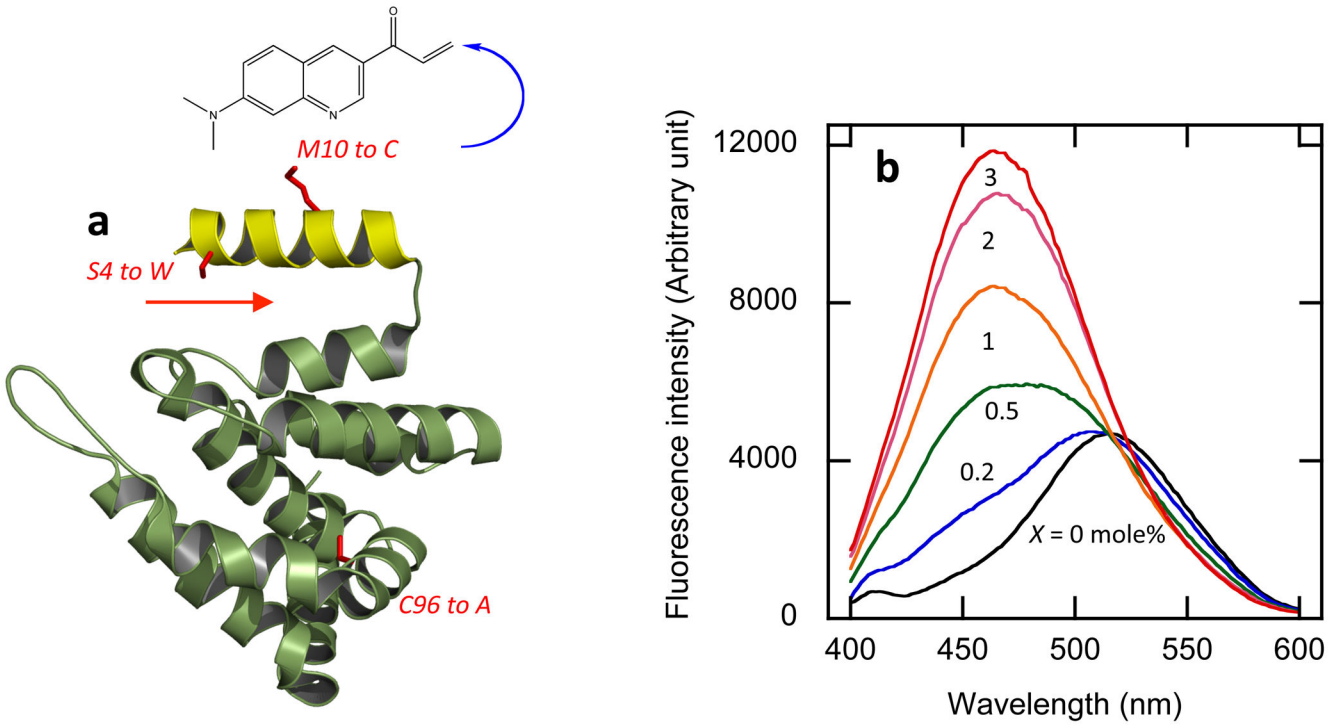

Fig 1.

Structure and spectral properties of the PtdIns(4,5)P_2 sensor, *DAN-eENTH*. (**a**) The crystal structure[20] of the epsin 1 ENTH is shown with mutated residues highlighted in red and labeled. The N-terminal helix is shown in yellow and the single site of labeling by the DAN group is indicated by a blue curved arrow. The red arrow shows the location of PtdIns(4,5)P_2-binding site. (**b**) Fluorescence emission spectra of *DAN-eENTH* (500 nM) in the presence of phosphatidylcholine/phosphatidylserine/PtdIns(4,5)P_2 (80-*x*:20:*x*) vesicles. Numbers (*x*) indicate mole% of PtdIns(4,5)P_2. The spectra were obtained spectrofluorometrically with (single-photon) excitation wavelength set at 392 nm. *DAN-eENTH* exhibited a dramatic blue shift with the maximal emission wavelength changing from 520 to 460 nm upon binding to PtdIns(4,5)P_2-containing vesicles, suggesting that [PtdIns(4,5)P_2] can be determined by the ratiometric analysis at two wavelengths, e.g., 520 nm and 460 nm

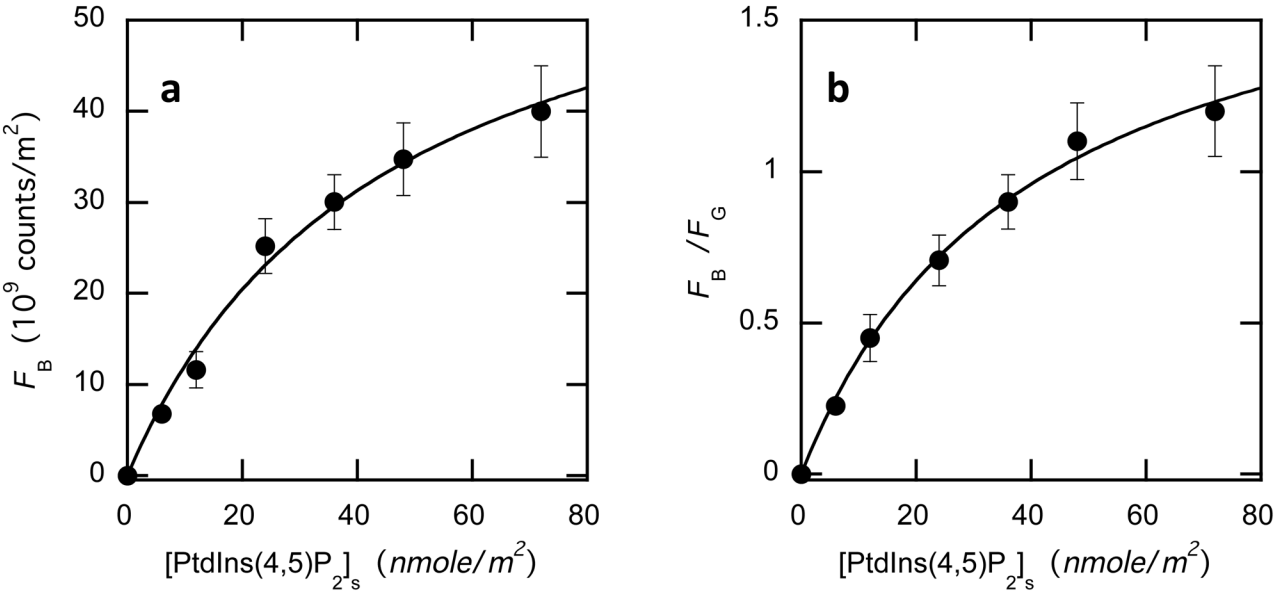

Fig 2.

In vitro PtdIns(4,5)P_2 calibration curves of *DAN-eENTH* for (**a**) single-channel and (**b**) ratiometric PtdIns(4,5)P_2 quantification. *DAN-eENTH* was two-photon excited at 780 nm by a two-photon microscope in the presence of phosphatidylcholine/phosphatidylserine/ PtdIns(4,5)P_2 (80-*x*:20:*x*) giant vesicles. F_B and F_G indicate blue and green channel (see the text for definition) fluorescence intensity, respectively. Non-linear least-squares analysis of the plot using the equation; F_B (or F_B/F_G) = $(F_B)_{max}$ (or $(F_B/F_G)_{max}$)/(1 + K_d/ [PtdIns(4,5)P_2]$_s$)[32] yields K_d and $(F_B)_{max}$ (or $(F_B/F_G)_{max}$) values and the calibration curves are constructed using these parameters. These calibration curves are then used to determine the PtdIns(4,5)P_2 concentration in cell membranes. Error bars indicate standard deviations calculated from >5 independent sets of measurements. Notice that (F_B/F_G) values are smaller than F_{450}/F_{520} in Fig. S3c because of the selection of our filter set.

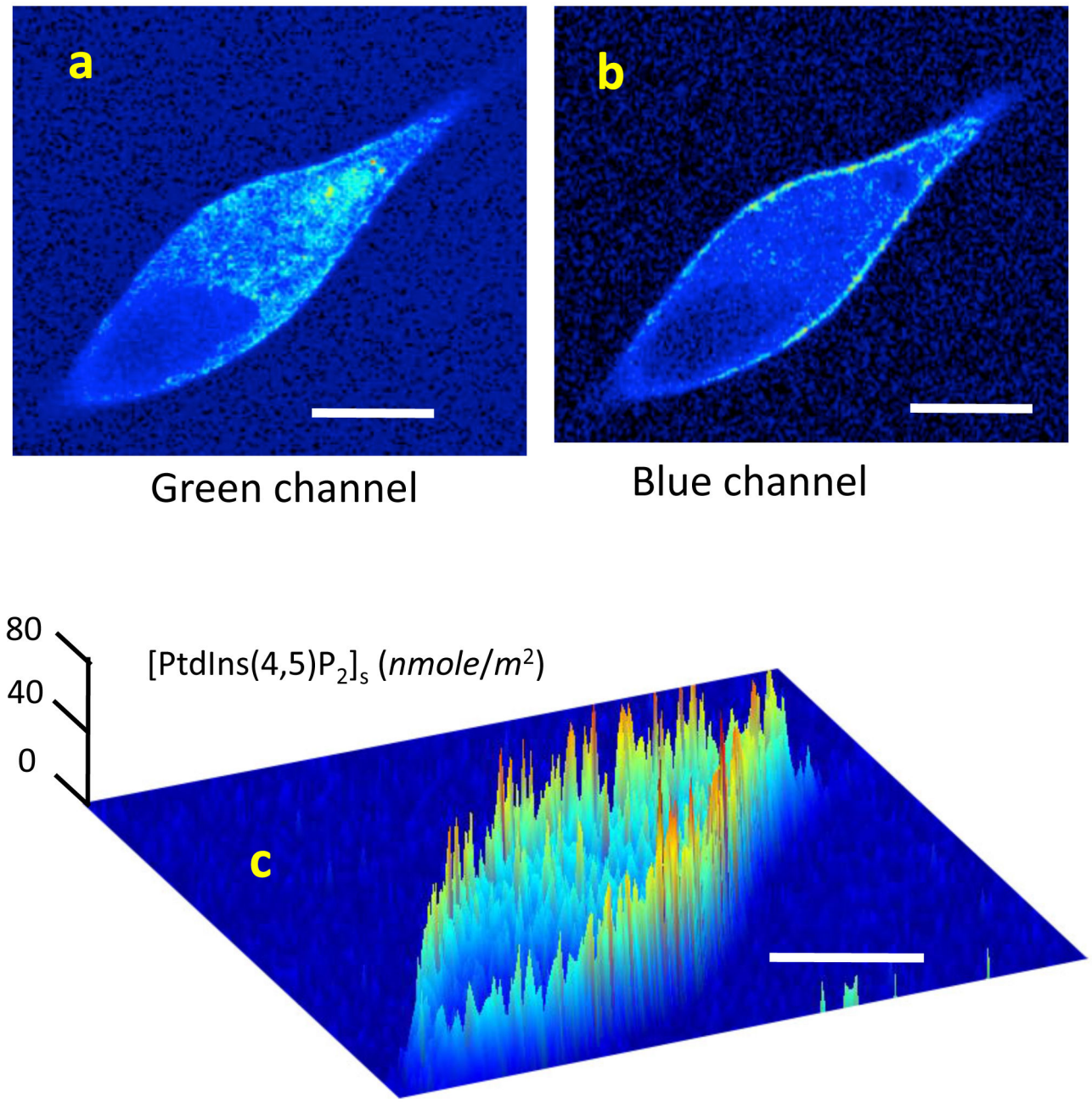

Fig. 3.

In situ quantification of PtdIns(4,5)P_2 in a representative NIH 3T3 cell by *DAN-eENTH*. (**a**) A green channel image representing the total sensor population (i.e., membrane-bound + free) shows cytosolic distribution of the *DAN-eENTH* sensor 10 minutes after microinjection. (**b**) A blue channel representing the membrane-bound sensor population shows predominant plasma membrane localization of the sensor. (**c**) Spatially resolved quantification of PtdIns(4,5)P_2 in the plasma membrane ($[PtdIns(4,5)P_2]_s$) by the ratiometric analysis of F_B/F_G using the calibration curve shown in Fig. 2b. Essentially the same result was obtained when F_B data were analyzed using the calibration curve shown in Fig. 2a.

Also, similar spatial heterogeneity and temporal fluctuation of PtdIns(4,5)P_2 in the plasma membrane were observed in >85% of 43 NIH 3T3 investigated. Pseudo-coloring is used for images with red indicating the highest concentration and blue the lowest. Bars indicate 5 μm. Lack of the sensor signal in the nucleus does not necessarily indicate the lack of PtdIns(4,5)P_2 in the nucleus because the *DAN-eENTH* does not translocate to the nucleus when microinjected to the cytoplasm due to the lack of a nuclear localization sequence. *DAN-eENTH* was two-photon excited at 780 nm. A 300x time-lapse video of temporal [PtdIns(4,5)P_2] fluctuation is shown in MovieS1.

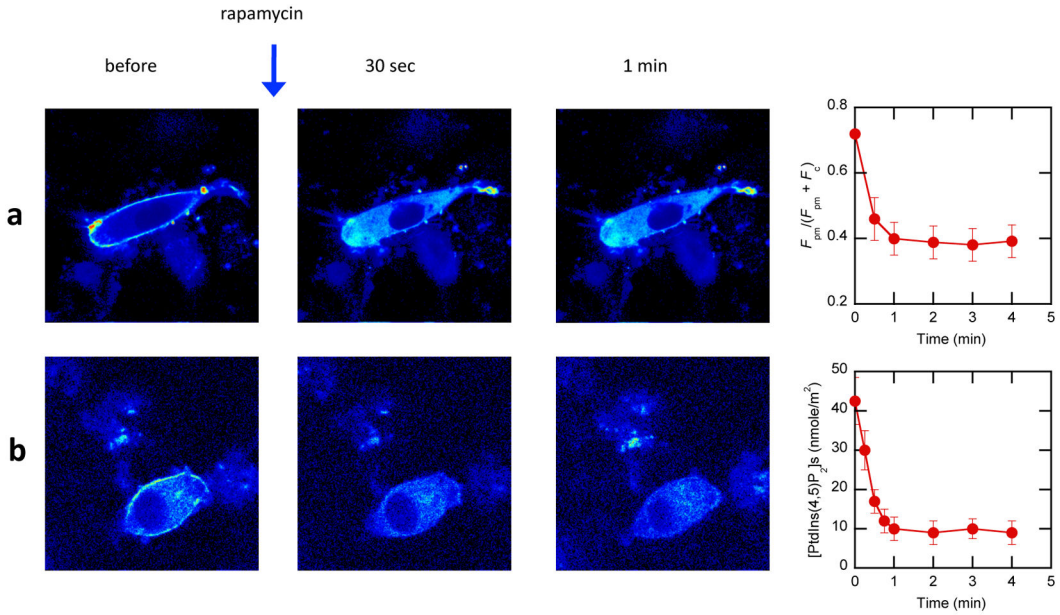

Fig. 4.

Monitoring PtdIns(4,5)P_2 decrease in NIH 3T3 cells by rapamycin-induced PtdIns(4,5)P_2 depletion system with (**a**) a conventional PtdIns(4,5)P_2 probe, PLCδ-PH-EGFP and (**b**) *DAN-eENTH*. After 2.5 μM rapamycin was added (blue arrow) to the cells, images were taken as a function of time. Representative images taken 30 seconds and 1 minute after the stimulation are shown here. The last column shows (**a**) the time course of relative population of PLCδ-PH-EGFP in the plasma membrane (see Supplementary Methods for calculation) and (**b**) the time course of spatially averaged $[PtdIns(4,5)P_2]_s$ in the plasma membrane. Error bars show standard deviation values from four measurements in four separate cells. Notice that under the same conditions, *DAN-eENTH* allows rapid quantification of dynamic [PtdIns(4,5)P_2] changes whereas PLCδ-PH-EGFP allows only qualitative or semi-quantitative estimation.

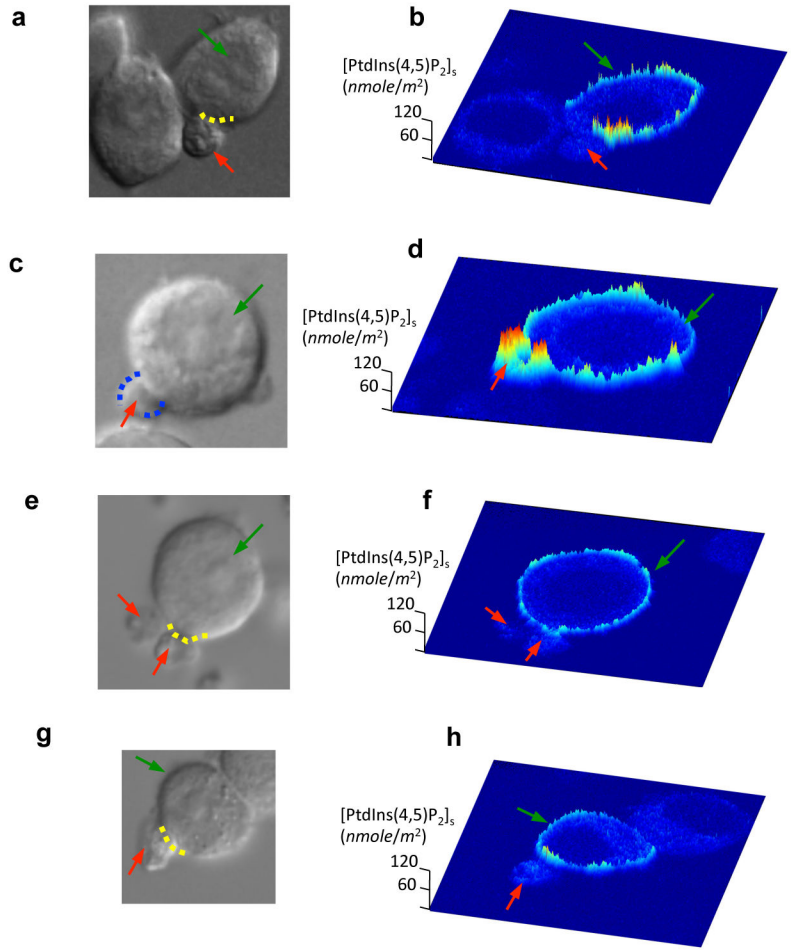

Fig. 5.

In situ quantification of PtdIns(4,5)P_2 in immune cells, macrophages, during phagocytosis (cell engulfing). (**a)** The differential interference contrast (DIC) image shows the contacts (yellow dotted lines) between Jurkat cells (red arrows) and macrophage J774A.1 cells (green arrows). (**b)** Ratiometric $[PtdIns(4,5)P_2]_s$ quantification for the engulfing macrophage as described in Fig. 3c. Notice that the PtdIns(4,5)P_2 sensor was injected only into the marked macrophage cell (not to the Jurkat cell). The Jurkat cell was subsequently phagocytosed by the macrophage when $[PtdIns(4,5)P_2]_s$ at the cell contact region was above a threshold value. **(c)** The DIC image of another macrophage at the later stage of phagocytosis and **(d)** $[PtdIns(4,5)P_2]_s$ quantification for the macrophage. Pronounced enrichment of PtdIns(4,5)P_2 is seen in the pseudopod that is indicated by blue dotted lines in the DIC iamge. The DIC images of two macrophages **(e, g)** that made contact with Jurkat cells but failed to phagocytose them because $[PtdIns(4,5)P_2]_s$ in their cell contact regions **(f, h)** were below the threshold value. All images are on the same scale. Cellular contact regions are marked with yellow dotted lines. *DAN-eENTH* was two-photon excited at 780 nm. Representative cells were selected from >50 macrophages monitored and the threshold $[PtdIns(4,5)P_2]_s$ values were calculated from these cells.